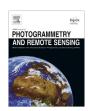
ELSEVIER

Contents lists available at ScienceDirect

# ISPRS Journal of Photogrammetry and Remote Sensing

journal homepage: www.elsevier.com/locate/isprsjprs



# Transformation of Landsat imagery into pseudo-hyperspectral imagery by a multiple regression-based model with application to metal depositrelated minerals mapping



Nguyen Tien Hoang a,b, Katsuaki Koike a,\*

- <sup>a</sup> Laboratory of Environmental Geosphere Engineering, Department of Urban Management, Graduate School of Engineering, Kyoto University, Katsura C1-2-215, Kyoto 615-8540. Japan
- <sup>b</sup> Department of Environmental Science, College of Sciences, Hue University, 77 Nguyen Hue, Hue, Viet Nam

### ARTICLE INFO

## Article history: Received 19 January 2017 Received in revised form 4 August 2017 Accepted 28 September 2017

Keywords:
Pseudo-band reflectance
Multiple linear regression
Bayesian model averaging
Hyperion image
Landsat ETM+ image
Cuprite

## ABSTRACT

Hyperspectral remote sensing is superior to traditional multispectral remote sensing in detailed spectral information but has limited spatial and temporal coverage. Those limitations require an innovative technique that can simulate hyperspectral imagery from multispectral imagery with global coverage, continuous acquisition, and a small number of bands. For this, a combination of Hyperion and Landsat 7 ETM+ images is a representative target. The present study develops a new method, Pseudo-Hyperspectral Image Transformation Algorithm (PHITA), for transforming Landsat 7 ETM+ imagery into pseudo-Hyperion imagery using correlations between Landsat and Hyperion band reflectance data. Each correlation is defined as a multiple linear regression model selected through Bayesian model averaging, in which Hyperion and Landsat bands are dependent and predictor variables, respectively. The resultant pseudo-image has a number of high-quality Hyperion bands of the same scene size as a Landsat image. Through verification of transformation accuracy by statistical analyses and surface mineral mapping, the pseudo-Hyperion image was proven very similar to the original band reflectances, because of large Pearson's correlation coefficients (generally > 0.94), small RMS error (mostly < 0.016), high structural similarity, and similar appearance of the color composite image. Using a reference mineral map built from an AVIRIS image and field surveys as ground truth, an advantage of the pseudo-image is clarified for the Cuprite hydrothermal alteration area in the western United States. The identification and mapping accuracies of metal deposit-related minerals were high even in areas outside the original Hyperion scene. Featured absorptions were reconstructed in pseudo-reflectance spectra of the typical minerals in the area. The results can enhance the potential of a large Landsat-series dataset over the long term by transformation into pseudo-Hyperion images for global land surfaces.

© 2017 International Society for Photogrammetry and Remote Sensing, Inc. (ISPRS). Published by Elsevier B.V. All rights reserved.

# 1. Introduction

Hyperspectral remote sensing can provide spectral information that is more detailed than multispectral remote sensing in many fields of application because of having hundreds of bands with high spectral resolution. This enables detailed discrimination of various types of Earth surface materials (Winter et al., 2007; Thenkabail et al., 2016). However, data resources of hyperspectral remote sensing are limited by both acquisition time and coverage area of the Earth surface. In contrast, multispectral remote sensing has

E-mail addresses: nguyen.hoang.44c@kyoto-u.jp (N.T. Hoang), koike.katsuaki. 5x@kyoto-u.ac.jp (K. Koike).

covered all areas for a long time, albeit using a small number of bands (Sun et al., 2015). Therefore, simulation of a hyperspectral image from a multispectral image is an innovative technique with which to compensate the disadvantages of each image type.

EO-1 Hyperion is a representative hyperspectral sensor, and its images have been applied to agriculture, forestry, environmental monitoring, and geological mapping (Galvão et al., 2005; Thenkabail et al., 2004; Rautiainen and Lukeš, 2015; Giardino et al., 2007; Kruse et al., 2003). The sensor covers the 0.4–2.5  $\mu m$  wavelength range with 242 bands, at  $\sim\!10$ -nm spectral resolution and 30-m spatial resolution (Miura et al., 2006). Despite having a greater number of bands with high spectral resolution, a Hyperion image scene is much narrower than a Landsat image for technical reasons (Table 1). In addition, the Landsat dataset has global

<sup>\*</sup> Corresponding author.

**Table 1**Data specifications of Landsat 7 ETM+ and EO-1 Hyperion images.

Parameters	Landsat 7 ETM+	EO1-Hyperion
Wavelength range Spectral resolution	0.4-2.4 μm <sup>a</sup> 60-260 nm	0.4–2.5 μm ~10 nm
Spectral resolution Spectral coverage	Discrete	Continuous
Number of bands	7	242 <sup>b</sup>
Swath width	185 km	7.5 km
Spatial resolution	30 m, PAN: 15 m	30 m
Temporal resolution	16 days	Variable

- <sup>a</sup> Excludes thermal bands.
- <sup>b</sup> Only 198 bands are calibrated.

coverage and the longest continuous space-based record of Earth's land, whereas Hyperion provides a discrete dataset with the aforementioned limitation. If a Landsat image can be successfully transformed into a Hyperion image, the latter pseudo-hyperspectral image should be useful to various remote sensing fields by incorporating the advantages of each image type.

The EO-1 satellite follows approximately one minute after Landsat 7 along the same ground track (Pearlman et al., 2001). Because of their similar orbits and same acquisition dates, the conditions of the atmosphere and solar illumination strength are almost the same between Hyperion and Landsat 7 images, except for a small difference in solar zenith angle (Zhao et al., 2010). Moreover, their same spatial resolutions (30 m) enable highly accurate coregistration of Hyperion-to-ETM+ images. These specifications mean the images obtained are appropriate for syntheses of Landsat 7 ETM+ bands from narrower Hyperion bands (Jarecke et al., 2001; Barry et al., 2002; Nikolakopoulos et al., 2008; Zhao et al., 2010), and additionally, they provided a reasonable trial for the inverse transformation of Landsat 7 ETM+ to Hyperion images in this study.

Several studies have succeeded in simulating a Hyperion image from a EO-1 ALI image (Liu et al., 2009; Chen et al., 2008) and CHRIS/PROBA image from a Landsat 7 ETM+ image (Berezowski et al., 2012). Their methods were a modified spectral response function derived from pixel-mixing principles (Chen et al., 2008: Berezowski et al., 2012) and a universal pattern decomposition method, which is a spectral unmixing approach (Liu et al., 2009). Because both used only standard spectral profiles to identify soil, water, and vegetation, it is difficult to produce a detailed classification map with different types of surface materials from simulated hyperspectral images. Other relevant methods include the Color Resolution Improvement Software Package (CRISP), which transforms a multispectral image into a synthetic hyperspectral image (Winter et al., 2007), and the Spectral Resolution Enhancement Method (SREM), which incorporates a spectral angle weighted minimum distance matching method into CRISP (Sun et al., 2015). SREM was applied to simulate a cropped AVIRIS image from a simulated Landsat TM image generated by spectral resampling of the original AVIRIS image, and a Hyperion image from an ALI image. However, neither CRISP nor SREM performed well for zones of heterogeneous material distribution within a scene. In addition, these previous studies verified their methods only for the overlap areas of hyperspectral and multispectral images. Therefore, as far as we know, there has been no simulation of a Hyperion image from a Landsat image and for an area outside the original scene.

Based on the background above, the present study develops a new method, Pseudo-Hyperspectral Image Transformation Algorithm (PHITA), to transform a Landsat 7 ETM+ (ETM+ hereafter) image into a pseudo-hyperspectral image. The latter is termed a pseudo-Hyperion image, and uses a correlation of band reflectances between ETM+ and Hyperion data. The fact that the ground spatial resolutions of these images are nearly identical facilitates the transformation without downscaling or upscaling problems.

The numbers of bands and scene size of the resultant pseudo-Hyperion image are equal to high-quality bands of Hyperion and a Landsat image, respectively. This advanced image aids more detailed identification of minerals and mineral deposit exploration than traditional multispectral remote sensing.

### 2. Methods

### 2.1. PHITA

Because the bandwidth of ETM+ is much wider than that of Hyperion (Table 1), band reflectance of ETM+ is regarded as a weighted sum of reflectances from several Hyperion bands. This idea has been used to synthesize an ETM+ band reflectance from Hyperion reflectances at narrow multiple bands in preceding studies (Jarecke et al., 2001; Barry et al., 2002; Nikolakopoulos et al., 2008) by deriving the weights from the relationship of the spectral responses between Hyperion and ETM+ bands. Therefore, a linear relationship might hold between an ETM+ band and each Hyperion band, whose wavelength ranges overlap fully or partially. Another linear relationship holds in reverse, which is found in the CRISP sharpening algorithm (Winter et al., 2007) that simulates a hyperspectral image (*Y*) from a multispectral image (*X*) using a simple linear transformation, e.g.:

$$\mathsf{GX} = \mathsf{Y} + \mathsf{r},\tag{1}$$

where G and r denote a filtering matrix and the Gaussian random error, respectively. The spectrum at each pixel occupies each column of the matrices X and Y. Under a condition that G is a global average optimization and is constant for all pixels in the overlap area between hyperspectral and multispectral images, it can be determined by a least squares calculation as (Sun et al., 2015):

$$G = YX^{\mathsf{T}}(XX^{\mathsf{T}})^{-1}. (2)$$

Then, a simulated hyperspectral spectrum can be expressed as

$$\begin{bmatrix} y'_{1(j)} \\ y'_{2(j)} \\ \vdots \\ y'_{A(j)} \end{bmatrix} = \begin{bmatrix} g_{1,1} & g_{1,2} & \cdots & g_{1,B} \\ g_{2,1} & g_{2,2} & \cdots & g_{2,B} \\ \vdots & \vdots & \ddots & \vdots \\ g_{A,1} & g_{A,2} & \cdots & g_{A,B} \end{bmatrix} \cdot \begin{bmatrix} x_{1(j)} \\ x_{2(j)} \\ \vdots \\ x_{B(j)} \end{bmatrix}$$
(3)

or

$$\vec{y'}_{A(j)} = G\vec{x}_{B(j)},\tag{4}$$

where  $\vec{y}_{A(j)}$  is the simulated hyperspectral spectrum with A bands and  $\vec{x}_{B(j)}$  is the given multispectral spectrum with B bands at pixel j. Finally, an element of  $\vec{y}_{A(j)}$  such as  $y_{1(j)}$  at band 1 can be derived by a form of multiple linear regression between the hyperspectral band 1 and all the multispectral bands as

$$y'_{1(j)} = g_{1,1} \cdot x_{1(j)} + g_{1,2} \cdot x_{2(j)} + \dots + g_{1,B} \cdot x_{B(j)}, \tag{5}$$

for which each row of G corresponds to a regression coefficient vector. Based on this concept, PHITA has been developed using a multiple linear regression model of the band reflectances, in which the Hyperion band is a dependent variable and the six ETM+ bands of visible-to-near infrared (VNIR) and shortwave infrared (SWIR) are predictor variables:

$$\rho_{ij}^{H}(\lambda) = \beta_{0i} + \beta_{1i} \cdot \rho_{1j}^{L}(\lambda) + \beta_{2i} \cdot \rho_{2j}^{L}(\lambda) + \beta_{3i} \cdot \rho_{3j}^{L}(\lambda) + \beta_{4i} \cdot \rho_{4j}^{L}(\lambda) 
+ \beta_{5i} \cdot \rho_{5i}^{L}(\lambda) + \beta_{6i} \cdot \rho_{6i}^{L}(\lambda) + \epsilon_{ij},$$
(6)

where  $\rho_{ij}^H(\lambda)$  represents the reflectance of the Hyperion band i and location (pixel) j;  $\beta_{0i}$  is the intercept for i;  $\beta_{1i}$ ,  $\beta_{2i}$ ,  $\beta_{3i}$ ,  $\beta_{4i}$ ,  $\beta_{5i}$ , and  $\beta_{6i}$  are unknown regression coefficients between the ETM+ bands

# Download English Version:

# https://daneshyari.com/en/article/6949275

Download Persian Version:

https://daneshyari.com/article/6949275

<u>Daneshyari.com</u>